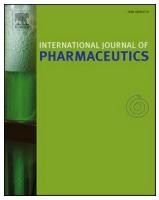
International Journal of Pharmaceutics 676 (2025) 125612



Contents lists available at ScienceDirect

International Journal of Pharmaceutics

journal homepage: www.elsevier.com/locate/ijpharm





Repurposing Chemotherapeutics in a Hyaluronic Acid-conjugate Combination Treatment Approach for the Local Immunomodulation of the Glioblastoma Microenvironment

Giulia Rodella [a,b], Zhanjun Ma [a], Bernard Ucakar [a], Nicolas Joudiou [b], Véronique Préat [a], Bernard Gallez [b,*], Alessio Malfanti [a,c,**]

[a] UCLouvain, Louvain Drug Research Institute, Advanced Drug Delivery and Biomaterials, Avenue Mounier 73 B1.73.12, 1200 Brussels, Belgium
[b] UCLouvain, Louvain Drug Research Institute, Biomedical Magnetic Resonance, Avenue Mounier 73 B1.73.08, 1200 Brussels, Belgium
[c] Departement of Pharmaceutical and Pharmacological Sciences, University of Padova, Via F. Marzolo, 5, 35131 Padova, Italy

ARTICLE INFO

Keywords:
Glioblastoma
Repurposing chemotherapeutics
Hyaluronic acid
Polymer therapeutics
Nanomedicines
Immunomodulation
Local treatment

ABSTRACT

The immunosuppressive tumor immune microenvironment (TIME) renders glioblastoma (GBM) refractory to current chemo-immunotherapeutics. We sought to explore a novel approach for local GBM-associated TIME immunomodulation based on a synergistic combination of the repurposed chemotherapeutic drugs doxorubicin (DOX), which acts to induce immunogenic cell death (ICD) and gemcitabine (GEM), which depletes immunosuppressive myeloid-derived suppressor cells (MDSCs). We conjugated DOX and GEM to hyaluronic acid (HA) to improve efficacy, given this polymer's ability to target CD44 which are overexpressed on cancer cells. The HA-DOX and HA-GEM polymer-drug conjugates provided synergistic cytotoxic effects and maintained ICD-related properties in GBM cells compared to a combination of free drugs. HA-DOX and HA-GEM also reverted the immunosuppressive GBM-associated TIME in orthotopic GL261 tumor-bearing mice by selectively depleting MDSCs and reprogramming M2-like macrophages towards a pro-inflammatory M1-like state, resulting in controlled tumor growth. Local HA-DOX and HA-GEM delivery also increased median survival and controlled tumor growth in an immune refractory SB28-GBM orthotopic mouse GBM model. These findings highlight the potential of repurposing clinically applicable chemotherapeutics in the context of polymer-drug combination treatments for novel immunomodulation strategies in unresectable GBM, which may open new avenues for developing innovative therapies.

1. Introduction

Glioblastoma (GBM, defined by the World Health Organization, as 'isocitrate dehydrogenase wild type GBM' Louis et al., 2021) is the most aggressive and common primary brain tumor in adults (Louis et al., 2016). The current standard of care involves maximal safe resection followed by radiotherapy and concomitant temozolomide (TMZ) treatment (Stupp et al., 2015). Surgery represents the central pillar of GBM management, with complete resection known to increase survival; however, a fraction of GBM patients are not eligible for surgery – the percentage may vary but it is generally around 10–20 % of the cases, owing to the tumor location in eloquent brain areas – and suffer from a worse prognosis (<8 months) (Serban et al., 2022; Lober-Handwerker et al., 2022). Therefore, we require novel therapeutic options for patients with unresectable GBM.

Cancer immunotherapy has attracted interest in oncology (Mellman et al., 2011), with several approaches currently undergoing preclinical and clinical investigations, including vaccines, immune checkpoint inhibitors, oncolytic viruses, and CAR T cell therapies (Majc et al., 2021); however, most GBM patients displayed negligible clinical responses attributed to a lack of T cell infiltration and the presence of an immunosuppressive tumor immune microenvironment (TIME) (Bausart et al., 2022b). Based on these considerations, localized immunomodulation might overcome immune dysfunction and prompt more successful

* Corresponding author.
** Corresponding authors at: UCLouvain, Louvain Drug Research Institute, Advanced Drug Delivery and Biomaterials, Avenue Mounier 73 B1.73.12, 1200, Brussels, Belgium.
E-mail addresses: bernard.gallez@uclouvain.be (B. Gallez), alessio.malfanti@unipd.it (A. Malfanti).

https://doi.org/10.1016/j.ijpharm.2025.125612
Received 8 January 2025; Received in revised form 15 April 2025; Accepted 15 April 2025
Available online 17 April 2025
0378-5173/© 2025 The Author(s). Published by Elsevier B.V. This is an open access article under the CC BY license (http://creativecommons.org/licenses/by/4.0/).

outcomes (Zhou et al., 2023). The TIME is characterized by the presence of tumor-associated myeloid cells (TAMCs) – myeloid cells with hematopoietic origins that include tumor-associated macrophages (TAMs) and myeloid-derived suppressor cells (MDSCs) (Sica et al., 2011) – that play a crucial role in dampening immune system responses by inhibiting innate and adaptive immunity and rendering GBM non-responsive to immunotherapies (Sica et al., 2011; Sampson et al., 2020; Gabrilovich and Nagaraj, 2009; Petty and Yang, 2017; Won et al., 2019). MDSCs – a heterogeneous population of bone marrow-derived immature cells subclassified into monocytic (M-MDSCs) and polymorphonuclear (PMN-MDSCs) – infiltrate GBM tumors and drive the suppression of antitumor immune responses. MDSCs accumulation in the GBM-associated TIME correlates with poorer outcomes, highlighting the importance of targeting this immunosuppressive cell type (Zhang et al., 2019a).

Treatment with chemotherapeutic drugs – a traditional approach for cancer cell eradication (Shurin, 2013) – actively impacts immune system responses (Shurin, 2013; Pusuluri et al., 2019). Repurposing clinically-approved drugs for immunomodulatory applications represents a potentially time- and cost-effective treatment strategy (Gonzalez-Fierro and Dueñas-González, 2021). The topoisomerase I inhibitor doxorubicin (DOX) induces immunogenic cell death (ICD) by inducing the release of 'eat me' signals (e.g., calreticulin [CRT] exposure and Interferon beta 1 [*INF-β*]/C-X-C motif chemokine ligand 10 [*CXCL10*] gene expression) involved in provoking dendritic cell maturation and consequent antigen presentation to adaptive T lymphocytes (Fucikova et al., 2020; Bezu et al., 2015; Amiri et al., 2023). Evaluations of intracranial DOX delivery in animal GBM models and human GBM clinical studies have provided encouraging results and suggested treatment safety (Lesniak et al., 2005; Voulgaris et al., 2002; Zhang et al., 2015; Chao et al., 2020); however, few studies have explored the impact of DOX on GBM-associated TIME (Chao et al., 2020; Arrieta et al., 2024). Additional chemotherapeutic drugs can directly affect specific immune cell populations; this includes gemcitabine (GEM) – a nucleoside analog of the antimetabolite deoxycytidine that can deplete MDSCs (Sasso et al., 2016). The evaluation of GEM in preclinical GBM studies as a monotherapy or in combination with other drugs/radiotherapy (due to its radio-sensitizing properties) has reported improved survival rates (Bastiancich et al., 2018). Of note, a combination of free DOX and GEM (DOX + GEM) in immune-refractory cancers such as triple-negative breast cancer demonstrated efficacy in tumor "re-education" by switching the TIME into an immunologically inflamed environment while depleting MDSCs, leading to superior T cell infiltration and cancer eradication (Sasso et al., 2016; Catania et al., 2023; Vogus et al., 2017). However, no studies evaluated the effects of this combination in GBM tumors, both as pure chemotherapeutics and their consequent effects on the immune response. Importantly, the blood–brain barrier hampers the penetration and diffusion of DOX and GEM throughout the brain, resulting in insufficient doses reaching the GBM tumor site and a lack of local immune responses (Chao et al., 2020; Noch et al., 2018; Nam et al., 2018; Zhao et al., 2020). Off-target chemotherapy-induced toxicity in healthy tissues represents an additional hurdle associated with systemic administration (Bush et al., 2019); however, localized chemo-immunomodulation can potentiate drug- and immune-related antitumor effects by overcoming the blood–brain barrier and minimizing off-target toxicities (Nam et al., 2018; Zhao et al., 2020). In this sense, the intracranial administration of drugs via convention-enhanced delivery (CED) establishes a pressure gradient that allows uniform drug distribution into the brain (Bastiancich et al., 2021).

In the hope of further improving therapeutic outcomes, studies have sought to reformulate drugs into polymer-based drug delivery systems as this approach *(i)* improves the physicochemical properties of the drugs (e.g., enhancing water solubility), *(ii)* provides specific cancer-targeting features, *(iii)* controls release over time, and *(iv)* improves the therapeutic efficacy of the drug (Rodriguez-Otormin et al., 2019; Ashford et al., 2021). Hyaluronic acid (HA) represents a widely used polymeric nanocarrier due to its biocompatibility and physicochemical properties (Kotla et al., 2021). HA has been extensively employed as a means to selectively target the CD44 receptor overexpressed on cancer cells (including GBM (Jiang et al., 2011) and, as such, reduce any harmful consequences on healthy tissues (Gupta et al., 2019).

In this study, we repurposed DOX and GEM as part of a novel combination chemo-immunomodulatory approach for the local treatment of unresectable GBM. We hypothesized that conjugating DOX and GEM to HA could improve TIME re-education by enhancing ICD and MDSCs depletion when administered in combination, thereby supporting better control over GBM tumor growth and extending the survival of GBM-bearing mice.

2. Materials and methods

2.1. Materials and reagents

Hyaluronic acid (HA, 100 kDa) was purchased from Lifecore Biomedical, LLC (Chaska, MN, USA); doxorubicin (DOX) and gemcitabine (GEM) were purchased from Chemielieva (JiangBei, China). 1-ethyl-3-(3-dimethylaminopropyl) carbodiimide (EDC), N-hydroxysuccinimide (NHS), 4-(4,6-dimethoxy-1,3,5-triazin-2-yl)-4-methylmorpholinium chloride (DMTMM Cl), paraformaldehyde (PFA), 2-(pyridyldithio)ethylamine hydrochloride, and crystal violet were purchased from Sigma-Aldrich (St. Louis, MO, USA). Ethylenediaminetetraacetic acid (EDTA), TRIzol™ reagent, Alamar blue, Calreticulin Recombinant Rabbit Monoclonal Antibody, and cell culture media and reagents were purchased from Thermo Fisher Scientific (Waltham, MA, USA). Zombie Aqua™ fixable viability dye was purchased from Biolegend (San Diego, CA, USA). Agarose, Tris borate EDTA (TBE), SybrSafe, and bovine serum albumin (BSA) were purchased from VWR International Srl (Leuven, Belgium). Endotoxin-free TE buffer was purchased from Qiagen (Hilden, Germany). GoScript™ Reverse Transcription Mix and Oligo (dT) GoTaq® qPCR Master Mix were purchased from Promega (Madison, WI, USA). XenoLight TM D-Luciferin potassium salt was purchased from Perkin Elmer (Shelton, CT, USA). Oligonucleotide primers were purchased from Integrated DNA Technologies (IDT) (Leuven, Belgium) and are listed in Supporting information (SI) (**Table S1**). The antibodies used and the provider are listed in **Table S2**.

2.2. Synthesis of HA-conjugates

HA-DOX was synthesized as previously described (Malfanti et al., 2022). For HA-GEM, HA (100 mg, 0.248 mmol, 1 eq.) was dissolved in 20 mL ultrapure water. After total HA dissolution, EDC (12.5 mg, 0.0812 mmol, 0.125 eq.) and NHS (7.5 mg, 0.066 mmol, 0.076 eq.) were added and stirred at room temperature for 1 h. GEM (15 mg, 0.056 mmol, 0.225 eq.) was then added to the mixture, and the reaction was stirred at 50 °C for 48 h. The mixture was primarily purified by ethanol precipitation (100 mL × 3) and then dialyzed against water (48 h). The final product was collected and desiccated under a vacuum and freeze-dried.

Yield(s): HA-DOX: 92 mg (%w/w DOX: 6.71 %, HA: 93.29 %);
HA-GEM: 84 mg (%w/w GEM: 1.41 %, HA: 98.59 %).

2.3. Physicochemical characterization of HA-conjugates

^{1}H NMR. Spectra were recorded on a Bruker Ultrashield Advance II 400 MHz instrument. HA-conjugates were diluted in deuterated water at 5 mg/mL.

Fourier-transform infrared spectroscopy (FT-IR). 5 mg HA-DOX and HA-GEM were mixed with approx. 40 mg KBr, and a pill was prepared. FT-IR analysis was recorded using Spectrum BX-PerkinElmer (San Diego, CA, USA) Instrument.

Drug loading. DOX loading was determined by UV–VIS spectroscopy at 488 nm, using a calibration curve produced with DOX solutions in the concentration range of 1–200 μg/mL (R^2 = 0.99). GEM content was

measured using ^{1}H NMR spectroscopy.

Size and zeta potential measurements. Dynamic light scattering (DLS) analyses were performed in triplicate using a Malvern Zetasizer ZS (Malvern, Cambridge, UK) equipped with a red laser (λ = 633 nm) at a fixed angle of 173° at 25 °C. HA-DOX and HA-GEM (0.5 mg/mL) were dispersed in 10 mM phosphate buffer containing 150 mM NaCl at pH 7.4 (PBS). Zeta potential values were measured by dissolving HA-DOX and HA-GEM in 1 mM KCl (2 mg/mL). Analyses were performed in triplicate.

2.4. In vitro studies

2.4.1. Cell lines

GFP-expressing murine glioma SB28 cells (DSMZ, German Collection of Microorganisms and Cell Cultures GmbH, Leibniz Institute, Braunschweig, Germany) and Rat gliosarcoma 9L cells (American Type Culture Collection, ATCC, Manassas, VA, USA) were grown in Dulbecco's Modified Eagle Medium (DMEM) with L-glutamine, 4.5 g/L D-glucose, and sodium pyruvate. Murine glioma GL261 cells (DSMZ, German Collection of Microorganisms and Cell Cultures GmbH, Leibniz Institute, Braunschweig, Germany) were maintained with Dulbecco's Modified Eagle's Medium (DMEM) with L-glutamine, 1 g/L D-glucose, and sodium pyruvate. Murine microglial BV-2 cells (American Type Culture Collection, ATCC, Manassas, VA, USA) were maintained in DMEM GlutaMAX with 4.5 g/L D-glucose.

All media were supplemented with 10 % fetal bovine serum (FBS), 100 U/mL penicillin, and 100 μg/mL streptomycin. SB28 and GL261 were incubated at 37 °C in a 10 % CO_2 atmosphere, while 9L and BV-2 cells were grown at 37 °C in a 5 % CO_2 atmosphere.

2.4.2. GBM cell viability

SB28, GL261, or 9L cells (5×10^3 cells/well) were seeded in 96-well plates and incubated for 24 h. Cells were treated with free DOX, free GEM, HA-DOX, HA-GEM, DOX + GEM, or HA-DOX + HA-GEM in the range of 0.0001–10 μM of DOX eq. concentrations with a 1:1 mol ratio DOX:GEM (**Fig. S1**). The solution of HA-conjugate was prepared with a desired concentration (μM) according to the % w/w and the molecular weight of the conjugated drug. After 72 h of treatment, cells were fixed with PFA (4 % v/v in water) and incubated with 50 μL/well crystal violet (0.5 % w/v in 20 % methanol v/v) at room temperature for 30 min. Plates were then rinsed three times with ultrapure water and left to dry overnight. Finally, cells were solubilized in methanol, and the absorbance (λ: 560 nm) was read with the SpectraMax ID5 microplate reader (Molecular Devices, San Jose, CA, USA). Assays were carried out in three independent experiments, and the data were normalized for the untreated group (100 % viability) and the Triton-X 100 group (0 % viability). IC_{50} values were calculated using a non-linear regression (curve-fit) mode, and Combination Indexes (CI) were calculated using the Chou-Talalay equation (1) (Chou, 2010).

$$x = \frac{IC50(drug1 + \boldsymbol{drug}2)}{IC50(drug2)} + \frac{IC50(\boldsymbol{drug}1 + drug2)}{IC50(drug1)} \quad (1)$$

2.5. Immunogenic cell death hallmarks

2.5.1. Calreticulin cell-surface exposure

SB28 cells (2×10^5 cells/well) were seeded in 12-well plates and maintained in a complete growth medium for 24 h. Cells were then treated with 0.1 μM (DOX concentration eq.) DOX, GEM, HA-DOX, HA-GEM, DOX + GEM, or HA-DOX + HA-GEM (ratio 1:1). After 24 h of treatments, flow cytometry (FACS) quantified viable cells positive for calreticulin (CRT). Cells were detached from the plate using trypsin-EDTA, washed three times with PBS, and suspended in PBS supplemented with 5 mg/mL BSA and 100 μL EDTA (0.5 M) (FACS buffer). Cells were stained with a primary anti-CRT antibody for 30 min at 4 °C, protected from light, and then treated with a secondary DyLight649-coupled antibody (DyLight™ 649 donkey anti-rabbit IgG, Biolegend, San Diego, CA, USA) for 30 min at 4 °C in the dark. Finally, data were acquired with Cytek® Aurora flow cytometer (Cytek Biosciences, Fremont, CA) and analyzed with FlowJo software (FlowJo, Ashland, OR, USA) with a gating strategy considering CRT-positive cells among viable GFP-expressing cells (**Fig. S3**).

2.5.2. Immunogenic cell death-associated cytokine gene expression

SB28 cells seeded (2×10^5 cells/well) in 12-well plates were treated with 0.1 μM (DOX concentration eq.) DOX, GEM, HA-DOX, HA-GEM, DOX + GEM or HA-DOX + HA-GEM (ratio 1:1). After 24 h of incubation at 37 °C, the quantitative measurement of *CXCL10* and *INF-β* relative gene expression was carried out with a real-time quantitative polymerase chain reaction (RT-qPCR). The cell medium was removed, and TRIzol™ Reagent (200 μL) and 40 μL chloroform were added to each sample. Cells were centrifuged at 12,000*g* for 15 min at 4 °C, and the mRNA contained in the water-soluble phase was precipitated in isopropanol and washed with 75 % ethanol solution. After drying, the mRNA pellet was dissolved in 10 μL endotoxin-free TE buffer, and the total concentration (ng/mL) was measured using a Nanodrop 2000 spectrophotometer (Thermo Scientific, USA). Reverse transcription of mRNA (0.33 μg/μL) was performed using GoScript™ Reverse Transcription Mix, Oligo dT (Promega, USA), and qPCR with GoTaq® qPCR Master Mix (primer sequences reported in **Table S1**). The relative mRNA expression was normalized to *RPL19* reference gene expression and calculated with the comparative method ($2^{-\Delta\Delta CT}$).

2.5.3. Pro-inflammatory and tolerance-associated cytokine expression and surface marker expression in microglial cells

BV-2 cells were seeded (2×10^5 cells/well) in 12-well plates and maintained in a complete culture medium for 24 h. Next, cells were incubated with BV-2 native medium supplemented with SB28-treated conditioned media (30:70 ratio). After 6 h of incubation, cytokine gene expression of pro-inflammatory (*TNF-α, IL-1β*, and *INF-β*) and tolerogenic markers (*Arginase* and *CD206*) was measured via RT-qPCR.

To study surface markers, cells were treated as described above, and flow cytometry analysis was performed by detaching cells from the plate using trypsin-EDTA, washing three times with PBS, and suspending in FACS buffer. Cells were stained with PE anti-mouse MHC II (I-A/I-E) and Brilliant Violet 421™ anti-mouse CD206 antibodies (MMR) (Biolegend, San Diego, CA, USA) for 30 min at 4 °C, protected from light. Finally, data were acquired with Cytek® Aurora flow cytometer (Cytek Biosciences, Fremont, CA) and analyzed with FlowJo software (FlowJo, Ashland, OR, USA).

2.6. In vivo studies

All experiments were performed following the Belgian national regulation guidelines and the EU Directive 2010/63/EU and were approved by the ethical committee for animal care of the Faculty of Medicine of the Université Catholique de Louvain (2023/UCL/MD/65). Animals had free access to water and food. Mice were monitored daily.

2.6.1. Orthotopic GL261 mouse model and localized treatments

Immunocompetent C57BL/6J mice (female, six weeks old), purchased from Charles River Laboratories (Wilmington, MA, USA), were orthotopically grafted with 1.5×10^5 GL261 cells/mouse (2 μL) in the right frontal lobe by CED using a Hamilton syringe (26S gauge needle) mounted on an infusion syringe pump (Harvard Apparatus, Holliston, MA, USA). Mice were anesthetized with an intraperitoneal injection of ketamine/xylazine (100 and 12 mg/kg, respectively) and positioned on a stereotactic frame. The injection was performed after drilling a hole into the skull with a surgical high-speed drill (Velleman, Gavere, Belgium) with the following coordinates: 2.1 mm lateral, 0.5 mm posterior from the bregma, and 2.6 mm deep from the outer border of the skull. The presence and volume of intracranial tumors were monitored by magnetic resonance imaging (MRI), as previously described (Bausart

et al., 2022a). MRI imaging confirmed tumor growth 9 days after GL261 orthotopic grafting. On day 10, mice were randomized according to the tumor size into three groups (n = 9) and treated via CED with DOX + GEM or HA-DOX + HA-GEM or left untreated. Treatments were administered at a dose of 5 μg DOX: 2.42 μg GEM (DOX: GEM molar ratio 1:1) in a 5 μL volume with a constant flow rate of 0.5 μL/min. Tumor growth was monitored on day 17 by MRI, and mice were euthanized on day 21 to assess the immune profile in the brain via FACS.

2.6.2. Antitumor activity analysis in the orthotopic SB28 mouse model

Immunocompetent C57BL/6J mice (female, six weeks old), purchased from Charles River Laboratories (Wilmington, MA, USA), were orthotopically grafted with 3×10^3 SB28 cells/mouse (2 μL) into the right frontal lobe by CED, following the same procedure described above. The presence and size of intracranial tumors were monitored by bioluminescence imaging using the IVIS Spectrum In Vivo Imaging System (Perkin Elmer, Waltham, MA, USA). For imaging, mice were anesthetized with inhaled isoflurane, intraperitoneally injected with D-luciferin (150 mg/kg), and imaged after 15 min. Obtained tumor sizes are expressed as total flux. Bioluminescence imaging confirmed the tumor presence 9 days after orthotopic SB28 cell grafting. On day 10, mice were randomized according to the tumor size into three groups (n = 7) and treated via CED with DOX + GEM or HA-DOX + HA-GEM or left untreated.

Treatments were administered at a dose of 5 μg DOX and 2.42 μg of GEM (DOX:GEM 1:1 drug eq. dose) in a 5 μL volume with a constant flow rate of 0.5 μL/min. Tumor growth was monitored over time by IVIS, and survival rate was assessed. Mice were euthanized according to the endpoints of 20 % body weight loss, 10 % body weight loss, and clinical signs of morbidity (lack of movement, paralysis, arched back). Brains were collected at the endpoints to evaluate the impact of the treatments on immune cells.

2.6.3. Flow cytometry analysis of the immune populations in brains

GBM-bearing brains were collected at specific time points or endpoints. Single-cell suspensions were obtained via mechanical dissociation and passage through a 70-μm cell strainer (Greiner Bio-One, Vilvoord, Belgium) and stored in a solution of FBS and 10 % DMSO at −80 °C until use. Before FACS analysis, cells were stained with a panel of antibodies (**Table S2**) for 30 min at 4 °C to quantify different cell populations. Samples were analyzed at Cytek® Aurora flow cytometer (Cytek Biosciences, Fremont, CA) by acquiring 20,000 events/samples and analyzed with FlowJo software (FlowJo, Ashland, OR, USA). Gating strategies are described in **Fig. S4**.

2.7. Statistical analyses

Statistical analyses were performed using GraphPad Prism (GraphPad Software Version 9.1.2, San Diego, CA, USA). Survival was plotted using Kaplan–Meier curves and analyzed with a log-rank (Mantel-Cox) test. Multiple comparisons were assessed via one-way ANOVA with Dunnett's multiple comparison tests. A difference of $P < 0.05$ was considered to indicate statistical significance. For *in vivo* studies, the power calculations were performed assuming a significance level (α) of 0.05 and 80 % power and a Cohen effect of 1.5 and assuming a 10 % loss due to unforeseen events.

3. Results

3.1. Synthesis and characterization of HA-based conjugates

We designed a strategy to conjugate DOX and GEM to HA (100 kDa Mw) and achieve drug synergism by locally and simultaneously administering them to GBM tumors. Our synthetic strategy is easily scalable and consists of linking DOX to HA via a pH-responsive linker through a HA-hydrazine intermediate and the DOX ketone group (Catania et al., 2023); GEM has been linked to HA via direct amide conjugation using an EDC/NHS strategy, exploiting the free amino group on the GEM pyrimidine ring (Fig. 1**A**). We purified HA-drug conjugates (HA-DOX and HA-GEM) by precipitation in ethanol and extended dialysis against water to remove any excess unconjugated drug.

We comprehensively characterized HA-DOX and HA-GEM via ^{1}H NMR and FT-IR, demonstrating purity and chemical identity. As demonstrated by NMR (Fig. 1**B**), the conjugation of DOX or GEM to HA resulted in the expected widening of characteristic drug signals (δ = 8.02–7.17 ppm, associated with the aromatic regions of DOX; δ = 7.75, 6.25 and 6.16 ppm, associated with the pyrimidine signals of GEM). We employed these signals to quantify the total drug content of HA-GEM (1.41 % w/w); alternatively, we determined the drug loading of HA-DOX via UV–Vis (6.71 % w/w) due to the overlap of the NMR spectra for HA and GEM. FT-IR analysis of HA-DOX and HA-GEM confirmed successful conjugation (Fig. 1**C**). For HA-DOX, we observed a shift in the stretching vibration of the amide group (—NH) associated initially with HA from 1508 to 1636 cm^{-1}, highlighting the formation of a new amide bond; moreover, the formation of π-π interactions reduced the stretching vibrations associated with hydroxyl groups (—OH) of HA (3400 cm^{-1}) due to the conjugation of DOX (more hydrophobic and planar), suggesting the formation of nanoaggregates. The FT-IR spectra of HA-GEM revealed a slight shift in the stretching vibration of the amide group (—NH) associated with HA from 1520 to 1540 cm^{-1}; moreover, the peak at 3400 cm^{-1} corresponding to the free amine group of the pyrimidine of GEM decreased, thus highlighting the involvement of this free amine in HA conjugation. Finally, we explored the size and zeta potential of HA-DOX and HA-GEM, which revealed a size of approximately 16 nm and a negative zeta potential (−21.4 mV for HA-DOX and −9.8 mV for HA-GEM) for both conjugates (Fig. 1**D**). Overall, our data support the chemical identity and purity of the synthesized HA-conjugates.

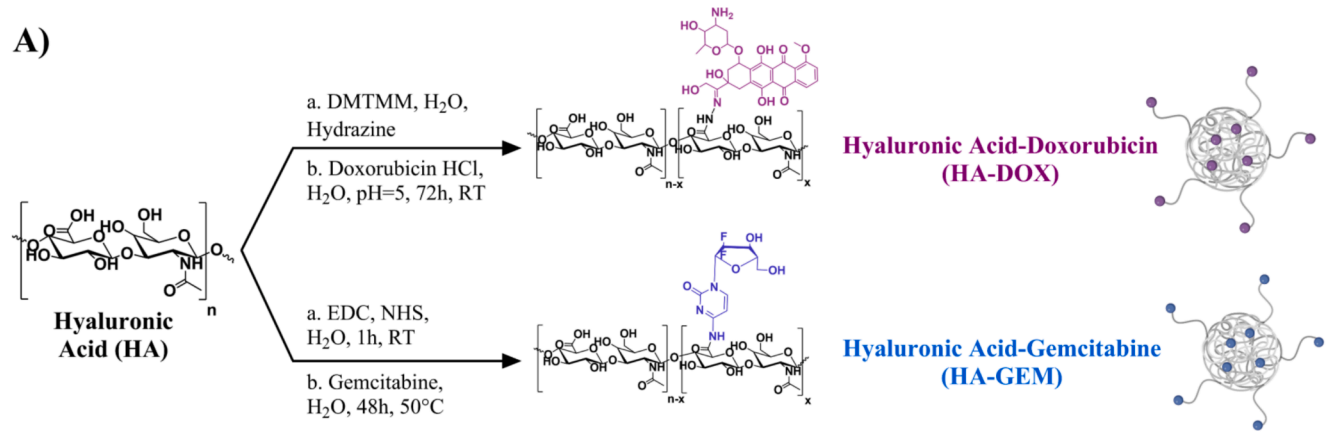
3.2. HA-DOX + HA-GEM provides a synergistic antitumor effect in GBM cells

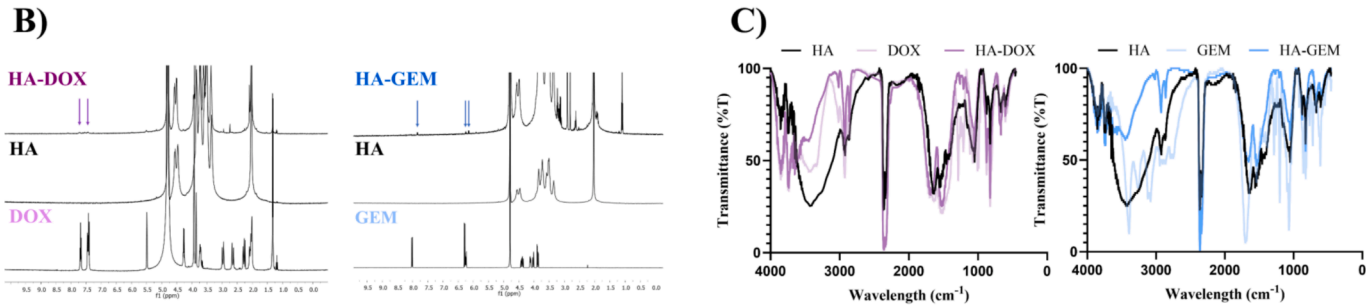
We investigated the antitumor activity of HA-DOX and HA-GEM alone or in combination in three glioblastoma cell lines: murine SB28 and GL261 cells and rat 9L cells. We employed a 1:1 M ratio for the combination treatment, identified by preliminary studies on DOX and GEM showing the lowest IC_{50}, compared to the other molar ratio tested (reported in **Fig. S1)**. We observed that HA-DOX + HA-GEM induced more significant cytotoxicity than HA-DOX, HA-GEM, or DOX + GEM (Fig. 2**A**); HA-DOX + HA-GEM displayed significantly decreased IC_{50} values (11.2 nM for SB28, ***$p < 0.0001$; 5.5 nM for GL261, **$p < 0.01$; and 11.0 nM for 9L, *$p < 0.05$) compared to DOX + GEM (20.6 nM for SB28; 8.4 nM for GL261; and 18.9 μM for 9L) (Fig. 2**B**). Analysis of combination index (CI) values revealed a significant synergistic inhibitory effect in SB28 and 9L cells (0.6022 for SB28, *$p < 0.05$ and 0.3517 for 9L, ****$p < 0.0001$) compared to DOX + GEM which displayed additive behavior in SB28 (1.1879) and 9L (0.8381) cells (Fig. 2**C**).

Overall, HA-DOX + HA-GEM induced higher cytotoxicity than DOX + GEM in mouse and rat GBM cell lines.

3.3. HA-DOX + HA-GEM treatment enhances the induction of immunogenic cell death and immunogenic behavior

Our previous study demonstrated that the conjugation of DOX to HA does not alter the ICD properties of the drug in GL261 GBM cells (Catania et al., 2023). Here, we explored ICD induction by DOX + GEM and HA-DOX + HA-GEM in an immune-refractory cell line such as SB28 to evaluate the role of GEM and HA-conjugation on ICD, given that GEM has no reported ICD-inducing function. As a first readout, we investigated CRT exposure on the membrane of SB28 cells and the expression of the *CXCL10* and *INF-β* relative genes as hallmarks of ICD (Fucikova et al., 2020).





D)

	Size (% number, nm)	Zeta Potential (mV)	Drug Loading (% w/w)
HA-DOX	15.9	-21.4	6.71
HA-GEM	16.0	-9.8	1.41

Fig. 1. Characterization of HA-DOX and HA-GEM. (A) Schematic representation and chemical formula of HA-DOX and HA-GEM. **(B)** ^{1}H NMR spectra of HA-DOX, HA, and DOX and HA-GEM, HA, and GEM. The arrows indicate the peaks associated with the aromatic region of DOX (δ = 8.02–7.17 ppm) and the pyrimidine signals of GEM (δ = 7.75, 6.25 and 6.16 ppm) conjugated to HA. **(D)** Table describing the physicochemical characterization results for HA-DOX and HA-GEM.

All treatments (0.1 μM; DOX, GEM, HA-DOX, HA-GEM, and combinations) induced a significant increase in the proportion of CRT-positive SB28 cells compared to the untreated (UT) control group (Fig. 3**A**). SB28 cells displaying exposed CRT underwent a 2-fold increase in all treatment groups (all ****p < 0.0001) except DOX (**p < 0.01). *INF-β* relative gene expression analysis highlighted the synergistic activity of combination therapies (Fig. 3**B**); while DOX or GEM treatment induced *INF-β* relative gene expression 18- and 139-fold compared to the untreated control, DOX + GEM supported a 330-fold increase relative to the untreated control (****p < 0.0001), suggesting a significantly greater induction of ICD. The increment of *INF-β* relative expression induced by GEM compared to UT has been reported by others in the literature (Hayashi et al., 2020). Likewise, HA-DOX or HA-GEM treatment induced *INF-β* relative expression by 35-fold and 124-fold compared to the untreated control, while HA-DOX + HA-GEM induced a 360-fold increase relative to the untreated control, again suggesting a significantly greater induction of ICD (****p < 0.0001, relative to the untreated control). Of note, DOX + GEM and HA-DOX + HA-GEM displayed a comparable ability to induce *INF-β* relative expression. Concerning *CXCL10*, all treatments induced a significantly higher expression of this hallmark of ICD when compared to the untreated group (Fig. 3**B**). Surprisingly, DOX and HA-DOX displayed less ability to induce *CXCL10* expression than GEM, HA-GEM, DOX + GEM, and HA-DOX + HA-GEM. These results might be explained by the higher CD44 expression on SB28 suggesting an HA-driven endocytosis (**Fig. S5**), in line with our previous findings with BV-2 microglia and GL261 GBM cells (Catania et al., 2023).

Next, we investigated the impact of single and combination therapies on microglial activation, aiming to explore the capacity of our treatment to trigger innate immunity (Quail and Joyce, 2017). We exposed murine BV-2 cells to conditioned media collected from pre-treated SB28 cells to explore the influence of released factors on immune cell activation (Fig. 3**C**). We observed that HA-DOX significantly increased the expression of pro-inflammatory marker genes (*TNF-α* and *IL-1β* but not for *INF-β*) compared to free DOX (TNF-α: DOX – 0.33-fold vs. HA-DOX – 3.99-fold, ****p < 0.0001; IL-1β: DOX – 9.94-fold vs. HA-DOX – 369.93-fold, *p < 0.05 with fold increases calculated compared to the untreated controls) (Fig. 3**C**). GEM and HA-GEM did not enhance the expression of pro-inflammatory marker genes while significantly enhancing Arginase as a tolerogenic factor compared to all other treatment groups (**p < 0.01). No differences on CD206 were observed. Finally, we discovered that HA-DOX + HA-GEM induced significantly higher levels of immunogenic marker gene expression than DOX + GEM (****p < 0.0001), although we saw no significant differences when

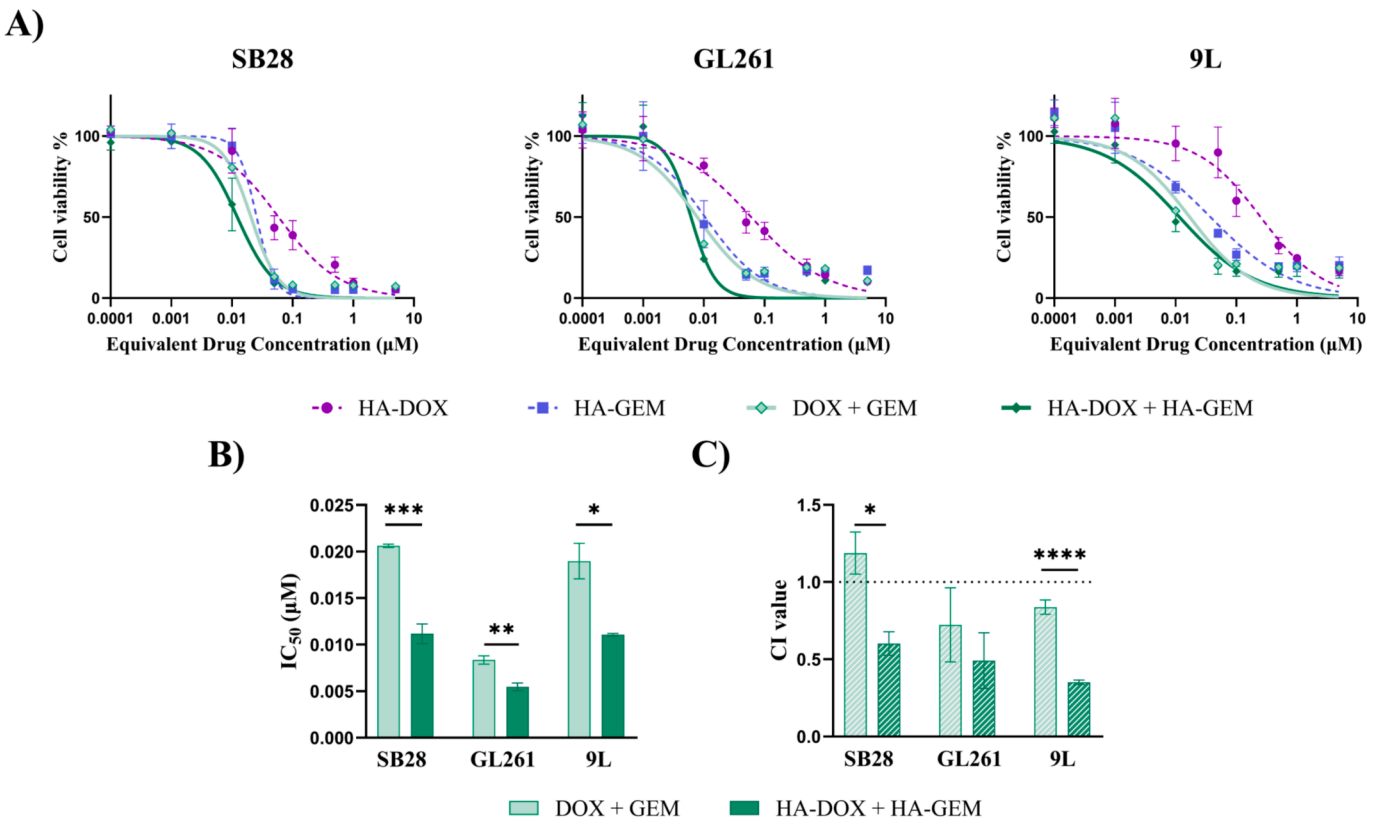


Fig. 2. Cytotoxicity of HA-DOX, HA-GEM, DOX + GEM, and HA-DOX + HA-GEM Treatments in GBM cells. **(A)** Cell viability curves after 72 h of incubation of SB28, GL261, and 9L cells with HA-DOX, HA-GEM, DOX + GEM, and HA-DOX + HA-GEM at a concentration range of 0.0001–10 μM DOX eq. (DOX: GEM molar ratio 1:1) (N = 3, n = 6). **(B)** IC_{50} values of DOX + GEM and HA-DOX + HA-GEM combination therapies calculated using non-linear regression (curve fit) in SB28, GL261, and 9L cells. **C)** Combination index (CI) values of DOX + GEM and HA-DOX + HA-GEM combination therapies calculated in SB28, GL261, and 9L cells. Statistical comparisons were performed using an unpaired *t*-test with Welch's correction. All values represent means ± standard deviation (SD) (*p < 0.05, **p < 0.01, ***p < 0.001, ****p < 0.0001).

analyzing tolerance marker gene expression. These data highlight how HA-conjugation may improve microglial activity through a combination drug anti-GBM approach (Fig. 3**C**).

We confirmed the immunogenicity/tolerance results using flow cytometry to detect the expression of the $MHCII^+$ (pro-inflammatory) and $CD206^+$ (pro-tolerance) cell surface markers in BV-2 cells (Fig. 3**D**). We observed an unbalanced MHCII:CD206 ratio indicative of a pro-inflammatory phenotype of BV-2 cells (low expression of CD206 in favor of high expression MHCII) when exposed to conditioned media from GBM cells treated with combination therapies (1.60-fold increase for DOX + GEM and 1.68-fold increase for HA-DOX + HA-GEM compared to the untreated control group, both ****p < 0.0001 compared to the untreated control), DOX (1.67-fold increase compared to the untreated control group, ****p < 0.0001), and HA-DOX (1.70-fold increase compared to the untreated control group, ****p < 0.0001). GEM and HA-GEM treatment did not significantly affect the MHCII: CD206 ratio compared to the untreated control group (Fig. 3**D**).

Overall, DOX, GEM, HA-DOX, and HA-GEM and their combinations induced ICD, as shown by increased CRT exposure and the expression of ICD-associated marker genes; however, only conditioned medium derived from GBM cells treated with DOX + GEM and HA-DOX + HA-GEM boosted the expression of immunostimulatory cytokines in microglia and induced microglial activation.

3.4. HA-DOX + HA-GEM treatment depletes monocytic MDSCs and controls tumor growth in GL261-bearing GBM model mice

Next, we explored the potential re-education of the TIME in GBM-bearing mice via TAMCs depletion after the CED-mediated administration of DOX + GEM and HA-DOX + HA-GEM. To this end, we orthotopically grafted mice with GL261 cells and intratumorally treated with DOX + GEM or HA-DOX + HA-GEM via CED on day 10 after tumor cell inoculation. We selected the administered dose (5 μg DOX and 2.43 μg GEM, drug equivalent dose) according to previous studies performed in our group (Catania et al., 2023); we analyzed the presence and location of induced tumors via MRI on days 9 and 17 and then sacrificed mice on day 21 to study the GBM-associated TIME (Fig. 4**A**). Analysis of tumor growth on day 9 (pre-treatment) revealed a similar level of tumor growth in all animals (Fig. 4**B**); subsequent analyses 7 days post-treatment (day 17 post-tumor inoculation) provided evidence that HA-DOX + HA-GEM induced a greater degree of tumor growth inhibition than DOX + GEM when compared to the untreated control group (Fig. 4**B**). No significant changes in body weight were observed (**Fig. S1B**). HA-DOX + HA-GEM induced a 52.1 % average decrease in tumor volume, while DOX + GEM induced a 27.8 % average decrease in tumor volume (Fig. 4**B**). However, no statistical difference between groups was observed.

On day 21 following tumor inoculation, we collected brains and evaluated changes in the TAMC cell populations (Fig. 4**C**). Only mice locally treated with HA-DOX + HA-GEM displayed a significant increment in the proportion of M1-like TAMs compared to the untreated control group (*p < 0.05); however, we observed a similar significant decrease in the proportion of M2-like TAMs following treatment with both DOX + GEM (*p < 0.05) and HA-DOX + HA-GEM (*p < 0.05) compared to the untreated control group. Interestingly, we observed a significant reduction in the proportion of M-MDSCs induced by HA-DOX + HA-GEM (but not DOX + GEM) compared to the untreated control (*p < 0.05). However, we failed to see any significant alterations in the

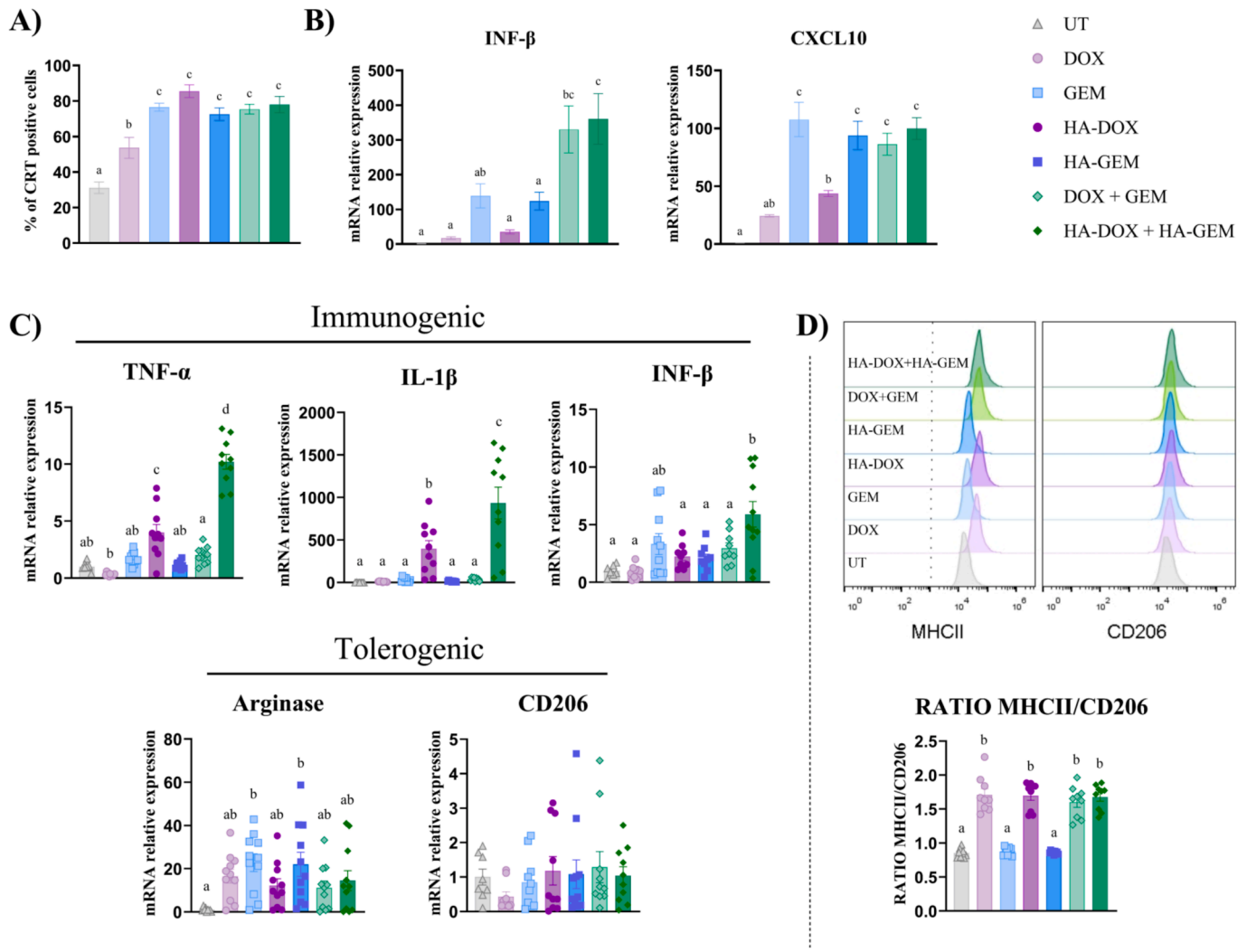


Fig. 3. Detection of immunogenic cell death hallmarks in SB28 GBM cells and immunogenic responses in microglia cells. **(A)** CRT exposure expressed as a percentage of CRT^+ cells among live cells (n = 3) following the exposure of SB28 cells to 0.1 μM DOX, GEM, HA-DOX, HA-GEM, DOX + GEM, and HA-DOX + HA-GEM for 24 h. **(B)** *INF-β* and *CXCL10* relative gene expression after SB28 cell treatment as described above. **(C)** TNF-α, IL-1β, *INF-β*, Arginase, and CD206 gene expression after a 6 h incubation of BV-2 cells with conditioned media from pre-treated SB28 cells (as described above). Untreated cells used as a reference; RPL19 used as a housekeeping gene (n = 3). **(D)** Representative graphs of expression of $MHCII^+$ and $CD206^+$ BV-2 cells and the ratio between MHCII/CD206 mean fluorescence intensities (MFI) after a 6 h incubation of BV-2 cells with conditioned media from pre-treated SB28 cells (described treatments). Values represent means ± standard deviation (SD). Statistical analyses performed with one-way ANOVA with Dunnett's multiple comparison tests (Data with different superscript letters are significantly different, $p < 0.05$).

proportion of PMN MDSCs. The ratio between monocytic/PMN MDSCs is 0.08 for DOX + GEM, 0.05 for HA-DOX + HA-GEM (*p < 0.05), and 0.09 for UT. These results support the hypothesis that repurposing chemotherapeutics as HA conjugates provides some benefit over the free drugs when combined. Our data also suggests that the immunomodulatory activity of HA-DOX + HA-GEM rewires the immune-refractory nature of the GBM-associated TIME towards a pro-inflammatory state. Unfortunately, this effect was not enough to provide an advantage in terms of survival when comparing the treatments (**Fig. S6**).

3.5. HA-DOX + HA-GEM controls the GBM growth and ameliorates the survival rate of SB28-GBM bearing mice

We finally explored the efficacy of DOX + GEM and HA-DOX + HA-GEM in a more immunosuppressive GBM model. We orthotopically grafted mice with SB28 cells and intratumorally administered DOX + GEM or HA-DOX + HA-GEM via CED at day 10 after tumor inoculation (Fig. 5**A**). For consistency, we used the same dose as in the previous model. Taking advantage of the intrinsic fluorescence of this model, we monitored GBM presence and location by IVIS on days 9, 14, and 17 and then evaluated mouse survival. We did not include standard of care (SOC) treatment as a control group since the SB28 model is known to be resistant to temozolomide (Genoud et al., 2021; Maeoka et al., 2023). In addition, this drug is known to induce immunosuppression which is counterintuitive for this work (Sengupta et al., 2012). HA-DOX + HA-GEM treatment maintained a smaller tumor size – although this failed to reach significance (p = 0.0549) – compared to DOX + GEM-treated or untreated mice (Fig. 5**B**). No decrease in body weight was observed, associated with no toxicity signs (**Fig. S2B**). Survival curves also revealed a trend (unfortunately, not reaching significance) towards improved survival with DOX + GEM treatment (28 days) and HA-DOX + HA-GEM treatment (32 days) compared to untreated mice (25 days) (Fig. 5**C**). At the experimental endpoint, we collected brains and evaluated changes in the TAMCs populations. While we failed to encounter any significant differences induced by HA-DOX + HA-GEM, a significant increase in the proportion of M2-like TAMs by DOX + GEM suggests that the HA-DOX + HA-GEM combination does not promote an immune-refractory TIME compared to the free drugs (Fig. 5**D**).

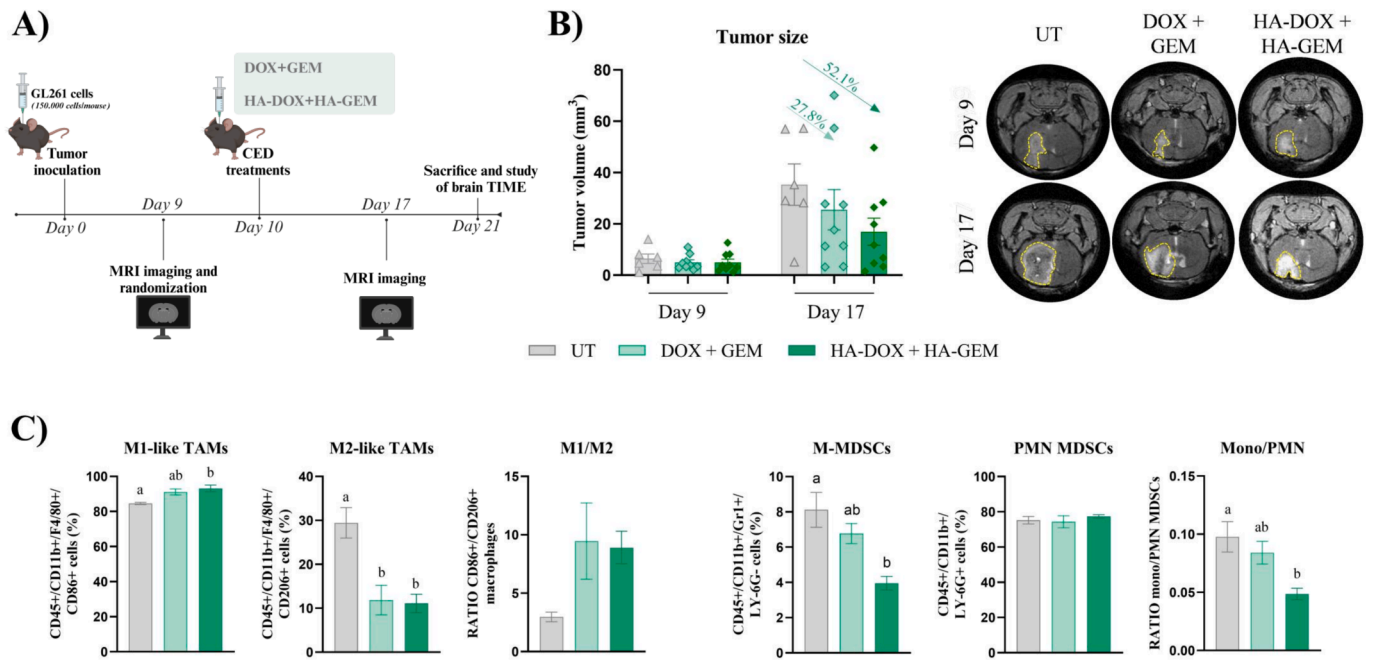


Fig. 4. The Local Administration of HA-DOX + HA-GEM by CED Depletes TAMCs and Controls Tumor Growth in GL261-bearing GBM Model Mice. (A) Schematic protocol for the intra-tumoral injection of DOX + GEM and HA-DOX + HA-GEM into GL261-bearing mice and subsequent analysis. (**B)** Analysis of tumor volume at days 9 (pre-treatment) and 17 (post-treatment) of the experimental time frame, measured by MRI with representative brain images shown. (**C)** FACS analysis of the cellular makeup of the GBM-associated TIME in the brain at day 21 (n = 9). Values represent mean ± SEM. Statistical analyses performed using one-way ANOVA with Dunnett's multiple comparison test. (Data with different superscript letters are significantly different, $p < 0.05$).

4. Discussion

The immunosuppressive TIME, systemic side effects, and a lack of therapeutically relevant doses at the tumor site have limited the success of systemically administered chemo- and immuno-therapies in unresectable GBM (Bausart et al., 2022b; Noch et al., 2018; Bush et al., 2019; Shaha et al., 2024). We hypothesized that the local administration of chemotherapeutics with inherent immunological activities linked to HA may induce an efficient antitumor-immune response with reduced off-target toxicity. Our polymer-based strategy combines two repurposed chemotherapeutics, DOX and GEM, conjugated to HA (100 kDa) at a synergistic ratio for the treatment of unresectable GBM (Amiri et al., 2023; Sasso et al., 2016; Eriksson et al., 2016) (Fig. 6). The novelty of our approach resides in revisiting the role of the chemotherapeutics that are not used only to kill cancer cells but also to immunomodulate the GBM-associated TIME by simultaneously activating the immune system and depleting M2-like TAMs and MDSCs (Kotla et al., 2021; Dalla Pieta et al., 2021; Tavianatou et al., 2019).

We synthesized HA-based conjugates using a cost-effective and easy scalable reaction, which we followed with robust purification by washing steps (including precipitation in ethanol and dialysis) that enabled the avoidance of time-consuming column purification. DOX conjugation through a pH-sensitive hydrazone linker supports the release of DOX from conjugates in the acidic GBM-associated TIME (pH < 3.4 in the 'necrotic zone,' <5.5 in the 'pseudo-palisading cell zone' and 6.2–7.0 in the 'cellular tumor zone') (Malfanti et al., 2022; Halcrow et al., 2019). As rapid DOX release could prompt uncontrolled inflammatory reactions, we hypothesized that conjugation with a bio-responsive linker could enhance the selective targeting of cancer cells while reducing undesired neurotoxicity, which might be supported by the lack of body weight during the treatment in both GBM models used that is usually a predictor of toxicity (Wang et al., 2016). On the other hand, GEM was linked through an amide bond. HA conjugates displayed a hydrodynamic diameter of ~20 nm for both conjugates, suggesting the presence of bulky aggregates that might favor GBM penetration and uniform distribution (Nance et al., 2014). The nanometric size of HA-conjugates stabilizes the drugs and prolongs their half-life in the tumor compared to free drugs, which might translate into an increase in anti-GBM activity *in vivo*. Moreover, the negative zeta potential of both HA-conjugates confers physiological stability (e.g., in cerebral spinal fluid) and better biocompatibility (Malfanti et al., 2022).

We employed SB28 cells to determine an optimal ratio between DOX and GEM and exploit any synergistic cytotoxic effect; a molar ratio of 1:1 prompted the synergistic inhibition of cell proliferation. Next, we investigated the cytotoxicity of HA-conjugates alone or in combination in three different high-grade glioma cell lines – GL261, SB28, and 9L – which mirror different patient groups. The GL261 murine model has been extensively used in the preclinical evaluation of immunotherapeutic approaches due to its well-characterized features and reproducibility (Haddad et al., 2021); however, this model remains susceptible to immune checkpoint inhibitors and may recapitulate the response of a few rare GBM patients (Genoud et al., 2018; Khalsa et al., 2020). The less immunogenic and poorly mutated SB28 model could better represent the immunotherapy sensitivity of most human clinical settings for translational purposes (Genoud et al., 2021). We included rat 9L cells, as they had been previously considered when investigating immunotherapeutic and cytokine treatments (Iwadate et al., 2005; Liu et al., 2007; Li et al., 2020). Our results describing the increased cytotoxicity of drug combinations compared to monotherapies align with previous reports in other "immunologically cold" cancer types (breast and ovarian tumors) (Vogus et al., 2017; Liu et al., 2014). Following HA-conjugation, both drugs retained their activity *in vitro* in all tested GBM cell lines; furthermore, the combination of HA-conjugates (HA-DOX + HA-GEM) appeared to display more significant cytotoxicity and synergism than the simple additive effect of the free drugs (DOX + GEM). This behavior remains crucial to target the highly heterogeneous nature of GBM through the different mechanisms of action of the drugs (Zhao et al., 2020; Lim et al., 2023); moreover, this approach could also be beneficial in the case of multidrug resistance established by GBM cells to circumvent chemo- and immuno-therapies (Zhao et al., 2020). Our findings

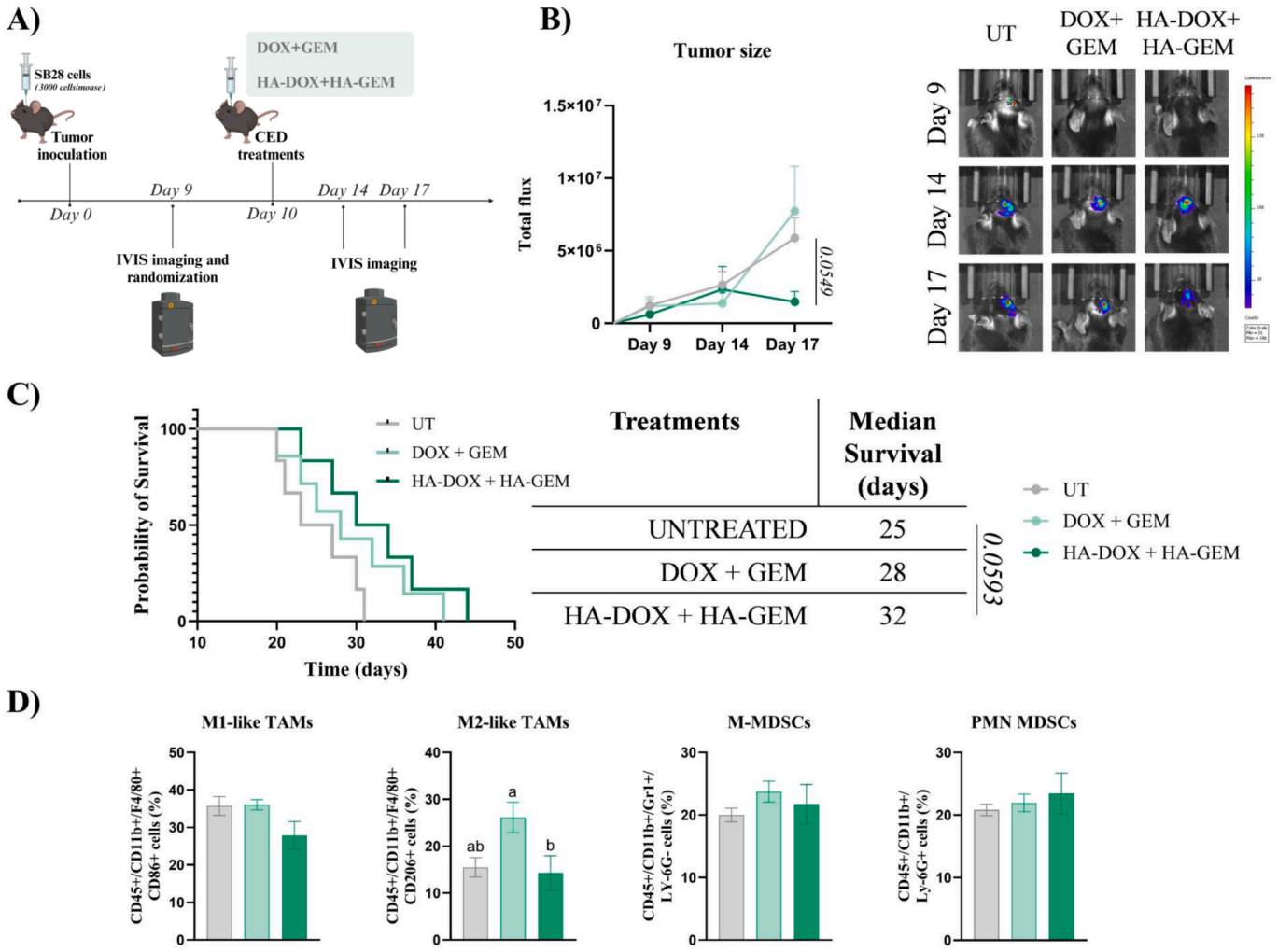


Fig. 5. ***In vivo*** **study of DOX + GEM and HA-DOX + HA-GEM treatment in an SB28 orthotopic GBM model. (A)** Schematic describing the intra-tumoral injection of DOX + GEM and HA-DOX + HA-GEM into SB28 tumor-bearing mice and the subsequent analytical approach. **(B)** Analysis of SB28 tumor volume via total flux measured by IVIS spectrum on days 9, 14, and 17 after tumor inoculation and representative IVIS images. **(C)** Kaplan-Meier survival curves for untreated (n = 6) and DOX + GEM- (n = 7), and HA-DOX + HA-GEM- (n = 6) treated mice, and a table describing median survival values. Data analyzed with a log-rank (Mantel-Cox) test. **(D)** FACS analysis of the cell makeup of the GBM-associated TIME at the experimental endpoint (n = 6/7). Values represent means ± SEM. Statistical analyses performed using one-way ANOVA with Dunnett's multiple comparison test. (Data with different superscript letters are significantly different, $p < 0.05$).

agree with a similar study demonstrating that polymer-based multidrug targeting leads to improved synergistic behavior; DOX and GEM encapsulated in micelles induced enhanced synergism compared to a combination of free drugs in ovarian, breast, and hepatocarcinoma cancer cell lines (Liu et al., 2014). In our approach, HA binding the CD44 receptor would also prompt higher cell uptake and consequently increased cytotoxicity (as we previously revealed) (Catania et al., 2023; Malfanti et al., 2022; Chaudhry et al., 2021; Thummarati et al., 2022); moreover, the biological "stickiness" of HA may facilitate adhesion to cell membranes (He, 2010; Kobayashi et al., 2020).

GBM cells treated with ICD inducers like DOX or mitoxantrone can result in a remarkable increase in CRT exposure – a major ICD hallmark – that, together with other factors, could support immune cell infiltration and GBM elimination (Amiri et al., 2023; Catania et al., 2023; Bausart et al., 2023). Our data in SB28 cells agree with previous reports, revealing a significant increase in CRT exposure following treatment with HA-conjugates and free drugs (Catania et al., 2023). These findings have particular relevance, considering the immunosuppressive nature of this GBM model that promotes immune evasion and low mutational burden (Genoud et al., 2018). In this context, the conjugation of drugs to HA played a crucial role: HA-DOX prompted greater CRT exposure than DOX alone, which could support the hypothesis of faster HA-driven cell uptake and the induction of intracellular cascades (Catania et al., 2023; Kobayashi et al., 2020). Accordingly, a related study revealed that HA-DOX triggered significantly greater CRT exposure in leukemia cells *in vitro* than the free drug (Krishnan et al., 2022). We also observed an unexpected effect of GEM in eliciting ICD hallmarks despite being acknowledged as a non-ICD inducer (Hayashi et al., 2020). Importantly, our data agree with other reports describing an *in vitro-in vivo* mismatch of GEM immunological behavior; despite it being acknowledged as a non-ICD inducer, GEM is well known to induce the release of danger-associated molecular patterns (DAMPs), *in vitro* (Hayashi et al., 2020). The role of GEM may be ascribed to the simultaneous induction of inhibitory DAMPs (e.g., prostaglandin E2), leading to the suppression of macrophage function and a non-immunogenic appearance *in vivo* (Hayashi et al., 2020). Despite the unexpected activity of GEM, DOX + GEM or HA-DOX + HA-GEM did not affect DOX mechanisms, thus maintaining ICD-related properties (Malfanti et al., 2022). We observed the immune immunomodulatory behavior of HA-conjugates following BV-2 microglia exposure to conditioned media from pre-treated SB28 cells. We observed the highest immunogenic cytokine genes (e.g., TNF-α, IL-1β, and *INF-β*) expression when exposing microglia to conditioned medium from HA-DOX + HA-GEM-treated SB28 cells; moreover, HA conjugation ameliorated immune responses via the upregulation of the

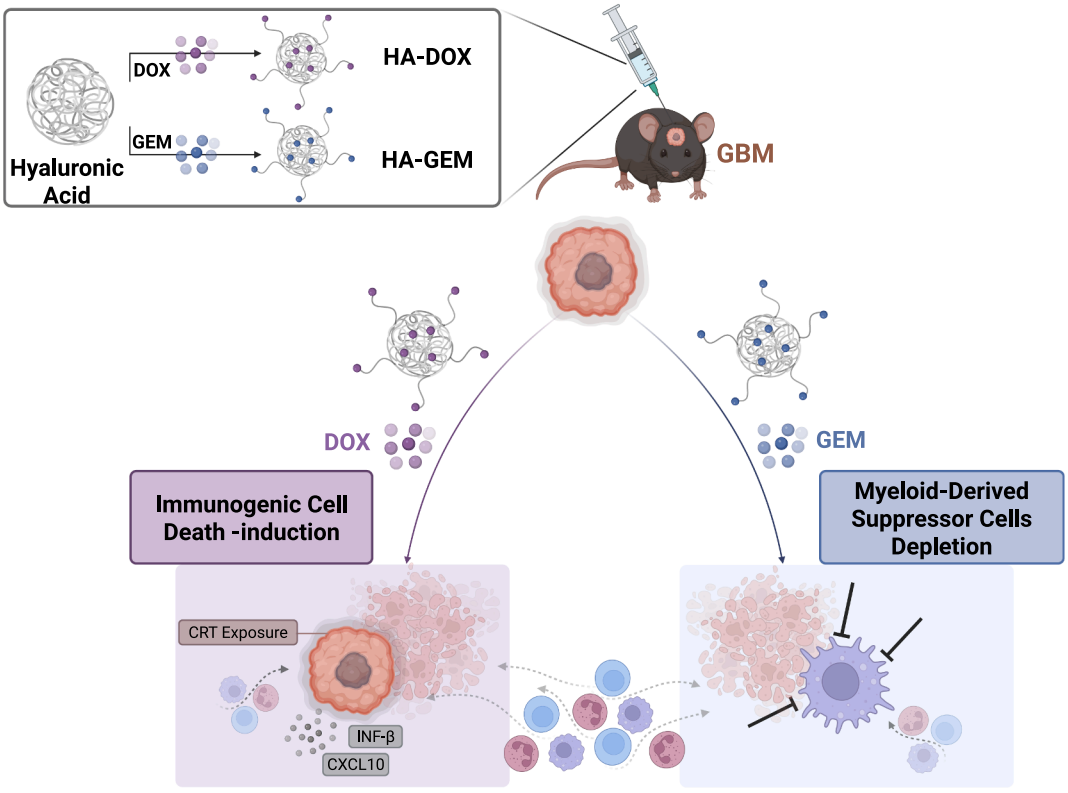


Fig. 6. Schematic representation of the proposed strategy. Doxorubicin (ICD inducer) and gemcitabine (MDSC depletion) have been used in a hyaluronic acid-conjugate combination treatment approach for the local immunomodulation of the glioblastoma microenvironment.

pro-inflammatory marker MHCII^{+}, consistently with the results obtained by Alaniz et al. (Alaniz et al., 2009). In this study, spleen dendritic cells from HA-treated mice displayed the increased expression of costimulatory signals (CD11c^{+}, MHCII^{+}, and CD80^{+}) that favored antigen presentation to effector T cells.

Due to the complex interplay between cancer and immune cells in the GBM-associated TIME and the lack of representative 2D/3D *in vitro* GBM models involving infiltrating TAMCs (Peereboom et al., 2019), we investigated the immunomodulatory activity of HA-conjugates *in vivo*. The effects of the individual drugs have already been investigated in other GBM models (Bastiancich et al., 2018; Catania et al., 2023). Due to ethical considerations, we did not assess the effects of the single conjugates in this study; in addition, in light of the *in vitro* studies, we speculated that their combined application may better reshape the GBM TIME landscape compared to the individual components. We treated immunocompetent GBM GL261-bearing mice characterized by the dynamic infiltration of immune cells and a peak number of TAMC presence at around day 21 following tumor inoculation (Ulasov et al., 2020). Our HA-based chemo-immunomodulating regimen induced significant changes in the TIME and, more specifically, in the TAMCs population via (*i*) the reduction of M2-like TAMs in favor of their pro-inflammatory counterparts and (*ii*) the depletion of M-MDSCs without impacting PMN-MDSCs. These findings agree with a previous study in our group highlighting the ability of HA-DOX in combination with an immune adjuvant (HA-CpG) to revert the TAM phenotype in orthotopic GL261-bearing tumors, which prompted improvements in long-term survival (Catania et al., 2023). HA-DOX + HA-GEM acted selectively on M-MDSCs, the most immune-suppressive subpopulation, to drastically reduce the proportion of these cells (Ren et al., 2023). This level of activity may be driven by the specific ability of GEM to inhibit M-MDSC infiltration in the tumor, as demonstrated by previous reports; for example, murine melanoma tumors (immuno-refractory in mice) treated with GEM displayed a reduced local number of MDSCs and a phenotypic switch from M2- to M1-like TAMs (Zhang et al., 2019b). Sasso et al. also demonstrated that treatment with GEM-lipid nanocapsules transiently reduced the level of M-MDSCs in lymphoma (Sasso et al., 2016). Interestingly, low doses of systemically administered capecitabine (belonging to the same family of drugs as GEM) in GBM patients significantly reduced the number of infiltrated M-MDSCs and induced remarkable changes in the TIME (Peereboom et al., 2019). In our study, M-MDSC depletion occurred following HA-conjugate treatment, which may relate to faster CD44-mediated cell uptake. Given the reduction in tumor growth following treatment with HA-DOX + HA-GEM, we speculate that immunomodulation may impact antitumor outcomes when combined with other therapeutics and warrants further investigation.

Notably, a growing body of evidence suggests that the immunogenic GL261 model does not fully recapitulate the immune features of human GBM (Genoud et al., 2018). For this reason, we sought to determine the effect of our treatment approach on a more immune-resistant GBM model – SB28 cells. We found that SB28 tumor-bearing mice treated with HA-DOX + HA-GEM displayed reduced tumor growth over time and a trend toward increased median survival compared to DOX + GEM-treated or untreated mice ($p = 0.0593$). These results agree with the results of studies using similar strategies applied in tumor models generally recognized as poorly T cell infiltrated (e.g., breast and prostate cancer). Indeed, a HA-DOX-GEM conjugate developed for breast cancer treatment improved tumor growth inhibition and reduced acute toxicity compared to the mixture of free drugs (Vogus et al., 2017). Lammers *et al.* also demonstrated that a polymer-based DOX-GEM nanomedicine more efficiently inhibited the growth of prostate tumors than free drugs, suggesting the critical role of the polymeric carrier in improving outcomes (Lammers et al., 2009). In our study, the lack of TIME changes in this model may be attributed to the incapacity of treatments to induce long-lasting immune responses (Wu et al., 2021). Of note, we observed an improvement in the median survival in a highly immune-suppressive and infiltrative GBM model, considering that only a single dose of

treatments has been applied without any resection; nevertheless, the insights gained here might represent a conceivable starting point for implementing combination therapies with other clinically relevant immunotherapeutic approaches, such as CAR-T cells (Brown et al., 2024).

5. Conclusion

We developed a novel approach to locally immunomodulating unresectable GBM by repurposing two chemotherapeutics, DOX and GEM, by conjugation to HA and combining them at a synergistic ratio. The FDA approval of all components employed in this study supports the clinical translation of HA-DOX and HA-GEM; furthermore, their preparation and scaling-up procedures remain simple and cost-effective. The encouraging results obtained with one single CED administration of HA-DOX + HA-GEM in two GBM models highlight the importance of considering the immune response as an additional factor that can be leveraged in treating GBM. In conclusion, our innovative strategy could open new avenues for the development of multimodal treatments involving immunotherapies.

CRediT authorship contribution statement

Giulia Rodella: Conceptualization, Investigation, Writing – original draft, Writing – review & editing. **Zhanjun Ma:** Formal analysis, Data curation. **Bernard Ucakar:** Formal analysis. **Nicolas Joudiou:** Formal analysis. **Véronique Préat:** Conceptualization, Writing – review & editing, Funding acquisition. **Bernard Gallez:** Conceptualization, Writing – review & editing, Funding acquisition. **Alessio Malfanti:** Conceptualization, Investigation, Writing – review & editing, Funding acquisition.

Declaration of competing interest

The authors declare that they have no known competing financial interests or personal relationships that could have appeared to influence the work reported in this paper.

Acknowledgments

G.R. is supported by the EuroNanoMed III consortium (RAIN). V.P. is supported by Fonds de la Recherche Scientifique—Fonds National de la Recherche Scientifique (FRS-FNRS, grant agreement nos. 33669945, 40003419). B.G. is supported by the EuroNanomed Project (FNRS R.8009.21). A.M. was supported by the Marie Skłodowska-Curie Actions for an Individual European Fellowship under the European Union's Horizon 2020 research and innovation program (grant agreement no. 887609) by an FRS-FNRS fellowship (grant agreement no. 40000747) (Belgium) and is currently the recipient of the STARS Starting Grant (STARS StG 2023) (Grant Number: MALF_STARS_MUR24_01) funded by the University of Padova (Italy) and has received funding from the European Research Council (ERC) under the European Union's Horizon Europe Research and Innovation Program (grant agreement no. 101163931-GLIOMERS). MRI was performed on the equipment of the Nuclear and Electron Spin Technologies (NEST) platform. The authors thank Nicolas Dauguet (De Duve Institute, Brussels, Belgium) for the support of flow cytometry analysis. The figures have been designed with Biorender.com.

Appendix A. Supplementary data

Supplementary data to this article can be found online at https://doi.org/10.1016/j.ijpharm.2025.125612.

Data availability

Data will be made available on request.

References

Alaniz, L., et al., 2009. *Low molecular weight hyaluronan inhibits colorectal carcinoma growth by decreasing tumor cell proliferation and stimulating immune response*. Cancer Lett. 278 (1), 9–16.
Amiri, M., et al., 2023. *Stimulators of immunogenic cell death for cancer therapy: focusing on natural compounds*. Cancer Cell. Int. 23 (1), 200.
Arrieta, V.A., et al., 2024. *Ultrasound-mediated delivery of doxorubicin to the brain results in immune modulation and improved responses to PD-1 blockade in gliomas*. Nat. Commun. 15 (1), 4698.
Ashford, M.B., England, R.M., Akhtar, N., 2021. *Highway to Success—Developing Advanced Polymer Therapeutics*. Adv. Therapeut. 4 (5).
Bastiancich, C., et al., 2021. *Rationally designed drug delivery systems for the local treatment of resected glioblastoma*. Adv Drug Deliv Rev 177, 113951.
Bastiancich, C., Bastiat, G., Lagarce, F., 2018. *Gemcitabine and glioblastoma: challenges and current perspectives*. Drug Discov. Today 23 (2), 416–423.
Bausart, M., et al., 2022a. *Combination of DNA Vaccine and Immune Checkpoint Blockades Improves the Immune Response in an Orthotopic Unresectable Glioblastoma Model*. Pharmaceutics 14 (5).
Bausart, M., et al., 2023. *Combination of local immunogenic cell death-inducing chemotherapy and DNA vaccine increases the survival of glioblastoma-bearing mice*. Nanomedicine 50, 102681.
Bausart, M., Preat, V., Malfanti, A., 2022b. *Immunotherapy for glioblastoma: the promise of combination strategies*. J. Exp. Clin. Cancer Res. 41 (1), 35.
Bezu, L., et al., 2015. *Combinatorial strategies for the induction of immunogenic cell death*. Front. Immunol. 6, 187.
Brown, C.E., et al., 2024. *Locoregional delivery of IL-13Ralpha2-targeting CAR-T cells in recurrent high-grade glioma: a phase 1 trial*. Nat. Med. 30 (4), 1001–1012.
Bush, N.A.O., Hervey-Jumper, S.L., Berger, M.S., 2019. Management of glioblastoma, present and future. World Neurosurg 131, 328–338.
Catania, G., et al., 2023. *Combination of hyaluronic acid conjugates with immunogenic cell death inducer and CpG for glioblastoma local chemo-immunotherapy elicits an immune response and induces long-term survival*. Biomaterials 294, 122006.
Chao, Y., Liang, C., Tao, H., Du, Y., Wu, D., Dong, Z., Jin, Q., Chen, G., Xu, J., Xiao, Z., Chen, Q., 2020. Localized cocktail chemoimmunotherapy after in situ gelation to trigger robust systemic antitumor immune responses. Sci. Adv. 6 (10), eaaz4204.
Chaudhry, G.E., et al., 2021. *Understanding Hyaluronan Receptor (CD44) Interaction, HA-CD44 Activated Potential Targets in Cancer Therapeutics*. Adv. Pharm. Bull. 11 (3), 426–438.
Chou, T.C., 2010. *Drug combination studies and their synergy quantification using the Chou-Talalay method*. Cancer Res. 70 (2), 440–446.
Dalla Pieta, A., et al., 2021. *Hyaluronan is a natural and effective immunological adjuvant for protein-based vaccines*. Cell Mol. Immunol. 18 (5), 1197–1210.
Eriksson, E., et al., 2016. *Gemcitabine reduces MDSCs, tregs and TGFbeta-1 while restoring the teff/treg ratio in patients with pancreatic cancer*. J. Transl. Med. 14 (1), 282.
Fucikova, J., et al., 2020. *Detection of immunogenic cell death and its relevance for cancer therapy*. Cell Death Dis. 11 (11), 1013.
Gabrilovich, D.I., Nagaraj, S., 2009. *Myeloid-derived suppressor cells as regulators of the immune system*. Nat. Rev. Immunol. 9 (3), 162–174.
Genoud, V., et al., 2018. *Responsiveness to anti-PD-1 and anti-CTLA-4 immune checkpoint blockade in SB28 and GL261 mouse glioma models*. Oncoimmunology 7 (12), e1501137.
Genoud, V., et al., 2021. *Treating ICB-resistant glioma with anti-CD40 and mitotic spindle checkpoint controller BAL101553 (lisavanbulin)*. JCI Insight 6 (18).
Gonzalez-Fierro, A., Dueñas-González, A., 2021. *Drug repurposing for cancer therapy, easier said than done*. Sem. Cancer Biol. 68, 123–131.
Gupta, R.C., et al., 2019. *Hyaluronic Acid: Molecular Mechanisms and Therapeutic Trajectory*. Front. Vet. Sci. 6, 192.
Haddad, A.F., et al., 2021. *Mouse models of glioblastoma for the evaluation of novel therapeutic strategies*. Neurooncol Adv 3 (1), vdab100.
Halcrow, P., et al., 2019. *Role of endolysosomes and pH in the pathogenesis and treatment of glioblastoma*. Cancer Rep. 2 (6).
Hayashi, K., et al., 2020. *Tipping the immunostimulatory and inhibitory DAMP balance to harness immunogenic cell death*. Nat Commun 11 (1), 6299.
He, C., et al., 2010. *Effects of particle size and surface charge on cellular uptake and biodistribution of polymeric nanoparticles*. Biomaterials 31 (13), 3657–3666.
Iwadate, Y., Inoue, M., Saegusa, T., Tokusumi, Y., Kinoh, H., Hasegawa, M., Tagawa, M., Yamaura, A., Shimada, H., 2005. Recombinant Sendai virus vector induces complete remission of established brain tumors through efficient interleukin-2 gene transfer in vaccinated rats. Clinical cancer research 11 (10), 3821–3827.
Jiang, D., Liang, J., Noble, P.W., 2011. *Hyaluronan as an immune regulator in human diseases*. Physiol Rev 91 (1), 221–264.
Khalsa, J.K., et al., 2020. *Immune phenotyping of diverse syngeneic murine brain tumors identifies immunologically distinct types*. Nat Commun 11 (1), 3912.
Kobayashi, T., Chanmee, T., Itano, N., 2020. Hyaluronan: metabolism and function. Biomolecules 10 (11), 1525.
Kotla, N.G., et al., 2021. *Recent advances and prospects of hyaluronan as a multifunctional therapeutic system*. J. Control Rel. 336, 598–620.
Krishnan, V., et al., 2022. *Hyaluronic Acid Nanoparticles for Immunogenic Chemotherapy of Leukemia and T-Cell Lymphoma*. Pharmaceutics 14 (2).

Lammers, T., et al., 2009. *Simultaneous delivery of doxorubicin and gemcitabine to tumors in vivo using prototypic polymeric drug carriers*. Biomaterials 30 (20), 3466–3475.
Lesniak, M.S., Upadhyay, U., Goodwin, R., Tyler, B., Brem, H., 2005. Local delivery of doxorubicin for the treatment of malignant brain tumors in rats. Antican. Res. 25 (6B), 3825–3831.
Li, X.L., et al., 2020. *A Hybrid Glioma Tumor Cell Lysate Immunotherapy Vaccine Demonstrates Good Clinical Efficacy in the Rat Model*. Oncol. Targets Ther. 13, 8109–8124.
Lim, X.Y., et al., 2023. *Biomimetic nanotherapeutics for targeted drug delivery to glioblastoma multiforme*. Bioeng. Transl. Med. 8 (3), e10483.
Liu, Y., et al., 2007. *TGF-beta2 inhibition augments the effect of tumor vaccine and improves the survival of animals with pre-established brain tumors*. J. Neurooncol. 81 (2), 149–162.
Liu, D., et al., 2014. *Micellar nanoparticles loaded with gemcitabine and doxorubicin showed synergistic effect*. Colloids Surf B Biointerf. 113, 158–168.
Lober-Handwerker, R., et al., 2022. *Defining the impact of adjuvant treatment on the prognosis of patients with inoperable glioblastoma undergoing biopsy only: does the survival benefit outweigh the treatment effort?* Neurosurg. Rev. 45 (3), 2339–2347.
Louis, D.N., et al., 2016. *The 2016 World Health Organization Classification of Tumors of the Central Nervous System: a summary*. Acta Neuropathol. 131 (6), 803–820.
Louis, D.N., et al., 2021. *The 2021 WHO Classification of Tumors of the Central Nervous System: a summary*. Neuro Oncol. 23 (8), 1231–1251.
Maeoka, R., et al., 2023. *Local administration of shikonin improved the overall survival in orthotopic murine glioblastoma models with temozolomide resistance*. Biomed. Pharmacother. 166, 115296.
Majc, B., et al., 2021. *Immunotherapy of Glioblastoma: Current Strategies and Challenges in Tumor Model Development*. Cells 10 (2).
Malfanti, A., et al., 2022. *Design of Bio-Responsive Hyaluronic Acid-Doxorubicin Conjugates for the Local Treatment of Glioblastoma*. Pharmaceutics 14 (1).
Mellman, I., Coukos, G., Dranoff, G., 2011. *Cancer immunotherapy comes of age*. Nature 480 (7378), 480–489.
Nam, L., et al., 2018. *Drug Delivery Nanosystems for the Localized Treatment of Glioblastoma Multiforme*. Materials (Basel) 11 (5).
Nance, E., Zhang, C., Shih, T.Y., Xu, Q., Schuster, B.S., Hanes, J., 2014. Brain-penetrating nanoparticles improve paclitaxel efficacy in malignant glioma following local administration. ACS nano 8 (10), 10655–10664.
Noch, E.K., Ramakrishna, R., Magge, R., 2018. *Challenges in the Treatment of Glioblastoma: Multisystem Mechanisms of Therapeutic Resistance*. World Neurosurg 116, 505–517.
Peereboom, D.M., et al., 2019. *Metronomic capecitabine as an immune modulator in glioblastoma patients reduces myeloid-derived suppressor cells*. JCI Insight 4 (22).
Petty, A.J., Yang, Y., 2017. *Tumor-Associated Macrophages: Implications in Cancer Immunotherapy*. Immunotherapy 9 (3), 289–302.
Pusuluri, A., Wu, D., Mitragotri, S., 2019. *Immunological consequences of chemotherapy: Single drugs, combination therapies and nanoparticle-based treatments*. J. Control Rel. 305, 130–154.
Quail, D.F., Joyce, J.A., 2017. *The Microenvironmental Landscape of Brain Tumors*. Cancer Cell 31 (3), 326–341.
Ren, R., et al., 2020. *The recent progress of myeloid-derived suppressor cell and its targeted therapies in cancers*. MedComm 4 (4), e323.
Rodriguez-Otormin, F., et al., 2019. *Envisioning the future of polymer therapeutics for brain disorders*. Wiley Interdisc. Rev. Nanomed. Nanobiotechnol. 11 (1), e1532.
Sampson, J.H., et al., 2020. *Brain immunology and immunotherapy in brain tumours*. Nat. Rev. Cancer 20 (1), 12–25.
Sasso, M.S., et al., 2016. *Low dose gemcitabine-loaded lipid nanocapsules target monocytic myeloid-derived suppressor cells and potentiate cancer immunotherapy*. Biomaterials 96, 47–62.
Sengupta, S., et al., 2012. *Impact of temozolomide on immune response during malignant glioma chemotherapy*. Clin. Dev. Immunol. 2012, 831090.
Serban, G., et al., 2022. *Prognostic Factors of Survival in Glioblastoma Multiforme Patients-A Retrospective Study*. Diagnostics (Basel) 12 (11).
Shaha, S., Rodrigues, D., Mitragotri, S., 2024. *Locoregional drug delivery for cancer therapy: Preclinical progress and clinical translation*. J. Control Rel.
Shurin, M.R., 2013. *Dual role of immunomodulation by anticancer chemotherapy*. Nat. Med. 19 (1), 20–22.
Sica, A., et al., 2011. *Origin and Functions of Tumor-Associated Myeloid Cells (TAMCs)*. Cancer Microenviron. 5 (2), 133–149.
Stupp, R., et al., 2015. *Maintenance Therapy With Tumor-Treating Fields Plus Temozolomide vs Temozolomide Alone for Glioblastoma: A Randomized Clinical Trial*. JAMA 314 (23), 2535–2543.
Tavianatou, A.G., et al., 2019. *Hyaluronan: molecular size-dependent signaling and biological functions in inflammation and cancer*. FEBS J. 286 (15), 2883–2908.
Thummarati, P., et al., 2022. *Comparative study of dual delivery of gemcitabine and curcumin using CD44 targeting hyaluronic acid nanoparticles for cancer therapy*. Journal of Drug Delivery Science and Technology 77.
Ulasov, I., et al., 2020. *Temporal and spatial modulation of the tumor and systemic immune response in the murine Gl261 glioma model*. Plos One 15 (4).
Vogus, D.R., et al., 2017. *A hyaluronic acid conjugate engineered to synergistically and sequentially deliver gemcitabine and doxorubicin to treat triple negative breast cancer*. J Control Release 267, 191–202.
Voulgaris, S., et al., 2002. *Intratumoral Doxorubicin in Patients With Malignant Brain Gliomas*. Am. J. Clin. Oncol. 25 (1), 60–64.
Wang, L., et al., 2016. *Doxorubicin-Induced Systemic Inflammation Is Driven by Upregulation of Toll-Like Receptor TLR4 and Endotoxin Leakage*. Cancer Res 76 (22), 6631–6642.
Won, W.J., et al., 2019. *Metabolic and functional reprogramming of myeloid-derived suppressor cells and their therapeutic control in glioblastoma*. Cell Stress 3 (2), 47–65.
Wu, D., et al., 2021. *Gemcitabine and doxorubicin in immunostimulatory monophosphoryl lipid A liposomes for treating breast cancer*. Bioeng. Transl. Med. 6 (1), e10188.
Zhang, X., et al., 2015. *Tumor tropic delivery of doxorubicin-polymer conjugates using mesenchymal stem cells for glioma therapy*. Biomaterials 39, 269–281.
Zhang, P., et al., 2019a. *Therapeutic targeting of tumor-associated myeloid cells synergizes with radiation therapy for glioblastoma*. Proc. Nat. Acad. Sci. 116 (47), 23714–23723.
Zhang, Y., et al., 2019b. *Gemcitabine nanoparticles promote antitumor immunity against melanoma*. Biomaterials 189, 48–59.
Zhao, M., et al., 2020. *Nanocarrier-based drug combination therapy for glioblastoma*. Theranostics 10 (3), 1355–1372.
Zhou, S., et al., 2023. *Reprogramming systemic and local immune function to empower immunotherapy against glioblastoma*. Nat. Commun. 14 (1), 435.